Supporting Information

Advanced ternary ion-pair redox electrolytes for direct-contact dye-sensitized solar cells under one-sun and ambient lighting

Shanmuganathan Venkatesan,[a†] Hsiao-Ching Wang,[a†] Zi-Yan Liu,[a] Hsin Chen,[a] Hsisheng Teng,[ac] and Yuh-Lang Lee*[ab]

[a]Department of Chemical Engineering, National Cheng Kung University, No. 1, University Road, Tainan City 70101, Taiwan, E-mail: yllee@ mail.ncku.edu.tw

[b]Center for Resilience and Intelligence on Sustainable Energy Research (RiSER), National Cheng Kung University, Tainan 70101, Taiwan

† Shanmuganathan Venkatesan and Hsiao-Ching Wang contributed equally to this work

1. Experimental

1.1 Chemicals and Reagents

Fluorine-doped tin oxide glass (FTO) (TECTM7, SnO_2: F, 6–8 Ω/cm², 2.2 mm) was acquired from Quansheng Optical Technology Co., Ltd. Surlyn 1706 (30 μm) was obtained from Dupont, and Surlyn SX1170-25/60 (25/60 μm) was purchased from Solarnix. UV sealing agent and UV curing sealant (3035B) for DSSCs were sourced from OPAS UV Curing Corp. and Three Bond, respectively. Acetonitrile (ACN, CH_3CN, 99.9%) was sourced from Aencore Chemical Co., Ltd. Cobalt(II) chloride hexahydrate ($CoCl_2 \cdot 6H_2O$, 98%), 2,2'-Bipyridine (bpy, 98%), and nitrosyl tetrafluoroborate ($NOBF_4$, 98%) were obtained from Alfa Aesar. Titanium(IV) chloride ($TiCl_4$, 98%) and lithium perchlorate ($LiClO_4$, ≥ 95.0%) were sourced from Fluka. Titanium diisopropoxide bis(acetylacetonate) (TiAcAc, 75 wt.% in isopropanol), *tert*-butanol [$(CH_3)_3COH$, 99%], *4-tert*-butylpyridine (*tB*$_p$, $C_9H_{13}N$, 96%), and 3-methoxypropionitrile (MPN, >98%) were purchased from Sigma-Aldrich. Guanidine thiocyanate (GuSCN), lithium iodide (LiI, 99.0%), 1,2-dimethyl-3-propylimidazolium iodide (DMPII) and iodine (I_2, 99.9%) were also received from Sigma-Aldrich. DSL 30NR-D (main layer) and PST-400C (TiO_2 pastes) were provided by Dyesol PVT Ltd and JGC C&C (JGC catalysts and chemicals Ltd, Japan), respectively. Y123 dye and tris(4-methylphenyl) amine (TPAA, 99%) were supplied by Dyenamo (>98%). N719 dye (99%) and Surlyn films (SX 1170-25 and SX 1170-60) were received from Solaronix. All chemicals and solvents were used as received without further purification.

1.2 Preparation of the electrolytes and solutions

To further elucidate the interactions among the Co^{2+}/Co^{3+} redox couple, TPAA, and iodine species, CV titration experiments were carried out in ACN under identical supporting electrolyte conditions (0.1 M $LiClO_4$). The titration studies were performed in three sequential stages. In the

first stage, TPAA was incrementally added to the cobalt electrolyte (Co^{2+} 7.33 × 10^{-3} M and Co^{3+} 1.666 × 10^{-3} M), with TPAA concentration varied from ~10^{-5} to 10^{-3} M while maintaining constant cobalt concentration. In the second stage, I_2 was stepwise introduced into the pre-formed Co–TPAA system (TPAA 1.33 × 10^{-3} M), with concentrations ranging from ~10^{-6} to 10^{-3} M. In the third stage, LiI, 3.33 × 10^{-3} M was added to the Co–TPAA electrolyte, followed by incremental addition of iodine over a similar concentration range to generate polyiodide species (I_3^-) in situ. After each addition, the solutions were thoroughly mixed and deaerated prior to measurement. CV responses were recorded under identical experimental conditions, and variations in peak current and potential were monitored as a function of titrant concentration to evaluate interaction strength, charge-transfer behavior, and ion-pair formation within the system. In addition, ferrocene (Fc/Fc^+, 0.5 mM) was employed as an internal redox reference in all electrolyte solutions, providing a well-defined and reversible standard for reliable comparison and calibration of redox potentials.

Complementary to steady-state measurements, transient absorption spectroscopy (TAS) was employed to probe the charge-transfer dynamics of the same systems in ACN. Stock solutions of TPAA (1.0 × 10^{-3} M), $Co(bpy)_3^{2+}$ (1.0 × 10^{-3} M), $Co(bpy)_3^{3+}$ (1.0 × 10^{-3} M), and I_2 (1.0 × 10^{-3} M) were prepared, and working solutions (total volume 1.0 mL) were obtained by dilution. A reference solution containing TPAA (1.0 × 10^{-4} M) was used. Binary systems were prepared with TPAA (1.0 × 10^{-4} M) or cobalt species (Co^{2+} or Co^{3+}, 1.0 × 10^{-4} M) in combination with iodine (2.5 × 10^{-5} M). The Co–TPAA system contained TPAA (1.0 × 10^{-4} M) and cobalt species (1.0 × 10^{-4} M), while the ternary Co–TPAA–I system consisted of TPAA (1.0 × 10^{-4} M), Co^{2+} or Co^{3+} (1.0 × 10^{-4} M), and I_2 (2.5 × 10^{-5} M). All solutions were thoroughly mixed prior to measurement and analyzed under identical conditions. This systematic variation enabled direct comparison of excited-state dynamics and identification of intermediate species associated with charge transfer and ion-pair formation. The same concentration conditions were employed for photoluminescence (PL)

measurements to allow direct correlation between steady-state and transient spectroscopic results. For TAS measurements of dye-sensitized systems, TiO_2/Y123 electrodes were prepared using mesoporous TiO_2 films (~3 μm thickness) deposited on glass substrates and sintered following standard procedures. The films were sensitized with Y123 dye to achieve an absorbance of ~0.25–0.30 at 610 nm. For measurements, a thin layer of electrolyte was applied onto the sensitized film and covered with glass to ensure a uniform optical path without air bubbles. Control experiments were performed using an inert electrolyte ($NaClO_4$ (0.5 M) in ACN), while redox-active systems contained Co^{2+}/Co^{3+}, TPAA, and/or iodine species under conditions consistent with device-relevant electrolytes.

Nuclear magnetic resonance (NMR) measurements were performed in deuterated acetonitrile (CD_3CN) to investigate intermolecular interactions among the cobalt redox couple, TPAA, and iodine species. Stock solutions of TPAA (20 mM), $Co(bpy)_3^{2+}$ (20 mM), $Co(bpy)_3^{3+}$ (20 mM), and I_2 (20 mM) were prepared in CD_3CN. NMR samples were then obtained by appropriate dilution of the stock solutions to a final volume of 600 μL, yielding final concentrations in the range of 1.0 –2.0 mM depending on the system. The prepared samples included single-component solutions: TPAA (1.0 –2.0 mM), $Co(bpy)_3^{2+}$ (1.0 – 2.0 mM), and $Co(bpy)_3^{3+}$ (1.0 – 2.0 mM); binary mixtures: $Co(bpy)_3^{2+}$(1.0 –2.0 mM) and $Co(bpy)_3^{3+}$ (1.0 – 2.0 mM), $Co(bpy)_3^{2+}$ (1.0 – 2.0 mM) and TPAA (1.0 – 2.0 mM), $Co(bpy)_3^{2+}$ (1.0 – 2.0 mM) and I_2 (1.0 –2.0 mM), and TPAA (1.0 – 2.0 mM) and I_2 (1.0 – 2.0 mM); ternary systems: $Co(bpy)_3^{2+}$ (1.0 – 2.0 mM), $Co(bpy)_3^{3+}$ (1.0 – 2.0 mM), and TPAA (1.0 – 2.0 mM), as well as $Co(bpy)_3^{2+}$ (1.0 – 2.0 mM), TPAA (1.0 – 2.0 mM), and I_2 (1.0 – 2.0 mM); and a quaternary system containing $Co(bpy)_3^{2+}$ (1.0 –2.0 mM), $Co(bpy)_3^{3+}$ (1.0 –2.0 mM), TPAA (1.0 –2.0 mM), and I_2 (1.0 –2.0 mM). All samples were thoroughly mixed prior to transfer into NMR tubes. This concentration-controlled approach enabled systematic investigation of intermolecular interactions, ion-pair formation, and coordination behavior within the

TPAA..$Co(bpy)_3^{2+}$/$Co(bpy)_3^{3+}$...I_2 system, consistent with the UV–Vis and transient absorption spectroscopy studies.

1.3 Preparation of photoelectrodes

After cutting the FTO conductive glass to size, it was scrubbed with a neutral detergent, then cleaned in deionized water and acetone using ultrasonic agitation for 15 minutes, followed by blow-drying. The next step involved preparing CLs by two-step method to ensure a proper contact between the FTO and the main/scattering TiO_2 layers. In this method, the FTO was immersed in the $TiCl_4$ solution and heated to 70 °C for 30 min. After drying the $TiCl_4$ solution, TiAcAc solution was immediately sprayed (9 cycles) onto the dried FTO/$TiCl_4$ surface. Subsequently, the TiAcAc/$TiCl_4$-coated CS was annealed at 450 °C, resulting in the formation of highly dense and CLs. The thicknesses of the TiO_2 compact layers, prepared from TiAcAc/$TiCl_4$ precursors, was 45.95 nm. A 30 nm (Dyesol) titanium dioxide paste was manually screen-printed onto the pre-treated FTO glass, left to sit for 3 minutes to ensure a smooth surface, and then heat treated at 125°C for 6 minutes. Two layers, each about 2 μm thick, were applied, creating a main layer with small particle size and large surface area. Next, screen-printing was used to cover the main TiO_2 layer with 400 nm (CCIC) titanium dioxide paste, performing two screen-prints to achieve a total thickness of about 4 μm, forming a scattering layer. The titanium dioxide film was placed in a high-temperature furnace for sintering at 500°C through a segmented heating process to remove solvents and enhance contact between particles. After the porous titanium dioxide film was prepared, the $TiCl_4$ immersion treatment was repeated to grow tiny TiO_2 particles on the film, further increasing the dye adsorption surface area. The dye sensitizer used was 0.1 mM Y123 with 0.4 mM CDCA in a 1:1 (v/v) mixture of ACN and tert-butanol, where CDCA acted as a co-adsorbent to prevent dye stacking. For the N719 dye preparation, N719 dye (6 mg) was dissolved

in absolute ethanol (10 mL (0.986 mM), and the solution was stirred gently until the dye was completely dissolved. Before the sensitization procedure, the photoelectrode was cleaned with UV-Ozone for 15 minutes and heat treated at 450°C for 30 minutes to remove impurities. Once cooled to about 80°C, the photoelectrode was immersed in the dye solution in a dark environment for approximately 16 hours. After immersion, it was briefly rinsed with ethanol to remove excess dye and blow-dried with an air gun to complete the sensitization.

1.4 Preparation of counter electrodes

The FTO glass was first cut to the desired dimensions, and two holes were drilled diagonally at the corners of a 0.5 × 0.5 cm^2 square to serve as openings for electrolyte injection. After thorough cleaning of the drilled FTO substrates, Pt CEs were prepared by sputter-coating platinum onto the conductive surface. The sputtering process was carried out at a current of 40 mA for 105 seconds under a pressure of 1.0×10^{-2} Torr, resulting in a uniform Pt layer on the substrate. For the cyclic voltammetry measurements of electrolytes, the Pt deposited FTO was utilized as working electrodes.

1.5 Measurements

Cyclic voltammetry (CV) measurements were performed using a CH Instruments potentiostat (CHI627D, USA) with a three-electrode system at a scan rate of 100 mV s^{-1}. A platinum electrode was used as the counter electrode, an Ag/Ag^+ reference electrode served as the reference electrode, and a Pt/FTO electrode was used as the working electrode. Electrochemical impedance spectroscopy (EIS) was used to obtain the impedance spectra for the dummy cells, as well as sandwich and direct contact DSSCs with the electrolytes. From these spectra, key EIS parameters such as ion diffusion coefficients, ionic conductivity, charge transfer resistance at the counter electrode/electrolyte interface, capacitance, and recombination resistance were

determined. These measurements were carried out using a potentiostat equipped with an FRA module (PGSTAT30, Metrohm Autolab). For DSSCs, EIS data were collected in the dark under a controlled potential, applying a 10 mV AC sinusoidal signal across a frequency range of 100 mHz to 100 kHz. The EIS curves for both dummy cells and m-DSSCs were analyzed and fitted to suitable equivalent circuits, as depicted in Figure S2, using Z-view software. The calculated parameters were then used in the following equation to determine electrolyte conductivity: $\sigma = l / R_b A$,where l is the electrolyte thickness, A is the electrolyte's surface area, and R_b (bulk resistance) is derived from EIS data. The diffusion coefficient of the ions (D) is calculated using the limiting current density (J_{lim}) measured from the cyclic voltammetry curves. The related equation is $J_{lim} = 2nFCD/l$, where l = distance between the two electrodes, F = faraday constant, C = concentration of diffusion limiting species, and n = 1 (the number of electrons transferred in the redox reaction. Photovoltaic performance of the DSSCs was assessed using a digital source meter, scanning from 0 V to the open-circuit voltage under simulated one-sun conditions. Sunlight was simulated using a calibrated solar simulator (XES-301S, AM 1.5G, AAA class, San-Ei Electric) with a certified silicon reference cell. The J–V characteristics of the investigated DSSC were measured using a digital source meter, scanning from 0 V up to the corresponding open-circuit voltage under both sunlight and fluorescent-light conditions. Simulated sunlight was provided by a solar simulator (XES-301S, AM 1.5G, AAA class, San-Ei Electric) calibrated with a certified reference silicon cell. For indoor measurements, a custom-built system was used, enclosed with black curtains, and composed of an upper board, a lower platform, and a motorized lifter. Fluorescent tubes (TL5 Essential 14W/865, Philips), covered with woven wire meshes (20 mesh, Stainless Steel 304L), were mounted on the upper board. The mesh reduces light intensity to achieve moderate illuminances, while for higher illuminances, such as 7000 lux, the mesh was removed and the tubes positioned closer to the platform. The lifter allowed precise adjustment of the distance between the

board and the platform. Illuminances of 1000 lux and 7000 lux were achieved by positioning the tubes at approximately 33 cm (with three layers of wire mesh) and 21 cm (without any mesh) from the platform, respectively. Illuminance was verified using a digital light meter (YF-170, TENMARS ELECTRONICS), and the incident spectral irradiance was measured with a spectroradiometer (S-2440 model II, SOMA OPTICS). The PCEs of the cells under room light conditions were calculated using the following formula: $J_{sc} \times V_{oc} \times FF / P_{in} \times 100$. The UV-Vis absorption spectra of iodide, cobalt, TPAA, Co-TPAA-I redox species in ACN were determined using a Hitachi U-4100 spectrophotometer. The light sources comprised a deuterium lamp (< 345 nm) and a halogen lamp (< 345 nm, 50 W). redox couples in solvents were examined in quartz cuvettes with a light path of d = 1 cm. The reference spectrum of the solvents, utilized for dispersing redox couples, was measured and subtracted. Fluorescence measurements for these samples were conducted using a Hitachi F-7000 spectrometer. The instruments were equipped with double grating monochromators featuring a 300 nm focal length in both the excitation and emission paths. A xenon arc lamp (450 W) served as the white light source, and the emitted light from the redox couples was captured by a PMT detector fixed at a 90° angle relative to the excitation path. Dispersions of redox couples with comparable absorbance at 350 nm were recorded in quartz glass cuvettes. The incident photon-to-current efficiency spectra of the solar cell devices were detected using a xenon lamp-equipped quantum efficiency measurement system (QE-R3011, Enlitech, Taiwan) operating in DC mode. Nuclear magnetic resonance (NMR) measurements were performed to study the structural and electronic properties of TPAA and cobalt-based systems. All spectra were recorded in deuterated acetonitrile (CD_3CN) at room temperature. ^{1}H NMR spectra were acquired at 500 MHz, and ^{19}F NMR spectra at 470 MHz. Chemical shifts (δ) are reported in ppm and referenced to the residual solvent peak for ^{1}H and an external standard for ^{19}F. Samples were prepared at appropriate concentrations, transferred into 5

mm NMR tubes, and mixed thoroughly before analysis. Spectra were recorded with sufficient scans and processed using standard software. Peak assignments and spectral changes were used to evaluate molecular interactions, coordination effects, and ion-pair formation. Transient absorption spectroscopy (TAS) measurements were performed using a laser flash photolysis system (LP980, Edinburgh Instruments) equipped with a pulsed laser source, monochromator, and probe beam setup. Transient signals were detected using a fast photodetector and recorded as changes in absorbance over time. Samples were placed in a sample chamber and excited at wavelengths corresponding to the dye absorption. The system enables time-resolved analysis of charge-transfer and recombination processes, and all data were collected and analyzed using the instrument software under controlled conditions.

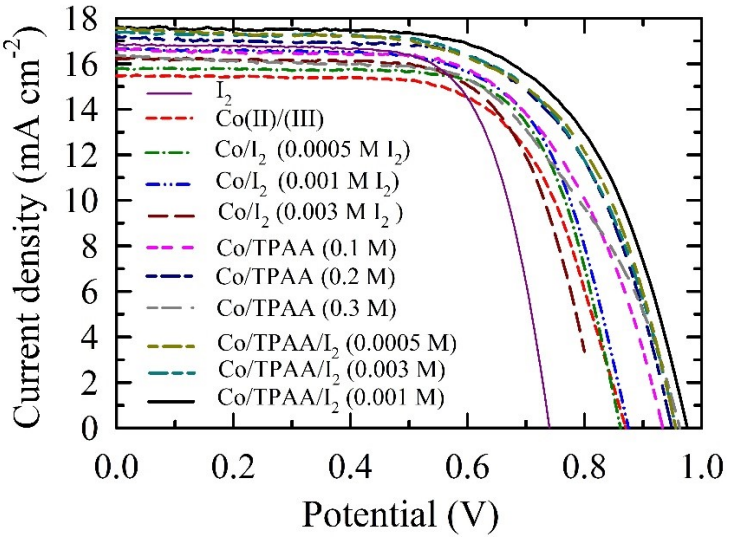

Figure S1. *J–V* curves of DSSCs with a sandwich structure using (i) iodide electrolytes, (ii) cobalt electrolytes, (iii) cobalt electrolytes with varying TPAA concentrations, and (iv) cobalt electrolytes containing the optimal TPAA concentration with different iodine concentrations.

Table S1. Cyclic voltammetry (CV) parameters, including anodic and cathodic peak potentials and peak currents, measured for the Co^{2+}/ Co^{3+}, I_2 (iodide/triiodide), Co/I_2, Co/TPAA, and Co/TPAA/I_2 redox species electrolytes in acetonitrile (ACN) using Pt working electrodes. The symbols * and # indicate the oxidation and reduction peaks, respectively, as shown in Figure 1.

System	Oxidation Peak (E_{pa}, V)	Oxidation Current (I_{pa}, A)	Reduction Peak (E_{pc} V)	$\Delta E_p = E_{pa} - E_{pc}$ (V)	Reduction Current (I_{pc}, A)
I_2 (1 redox peak)	0.247*	6.935×10^{-4}	0.116 #	0.131	-7.339×10^{-4}
I_2 (2 redox peak)	0.676*	2.757×10^{-4}	0.567#	0.109	-3.393×10^{-4}
Co^{2+}/ Co^{3+}	0.418*	1.834×10^{-3}	0.199#	0.219	-1.718×10^{-3}
Co/I_2 (1 redox peak)	0.434	1.141×10^{-3}	0.116#	0.318	-5.905×10^{-4}
Co/I_2 (2 redox peak)	0.709	9.753×10^{-5}	0.619#	0.090	-1.206×10^{-4}
TPAA (1 redox peak)	0.588*	3.586×10^{-4}	0.485#	0.103	-3.590×10^{-4}
TPAA (2 redox peak)	1.208*	3.702×10^{-4}	1.113#	0.095	$-1.155 \times 10^{-}4$
TPAA/I_2 (1 redox peak)	0.233*	3.440×10^{-4}	0.125#	0.108	-3.772×10^{-4}
TPAA/I_2 (2 redox peak)	0.630*	4.415×10^{-4}	0.484#	0.146	-3.595×10^{-4}
TPAA/I_2 (3 redox peak)	1.193*	3.461×10^{-4}	1.102#	0.091	-9.954×10^{-5}
Co/TPAA (1 redox peak)	0.454*	8.172×10^{-4}	0.165#	0.289	-1.346×10^{-3}
Co/TPAA (2 redox peak)	0.665*	1.600×10^{-4}	0.548#	0.117	-1.604×10^{-4}
Co/TPAA (3 redox peak)	1.269*	3.669×10^{-4}	1.171#	0.098	-1.007×10^{-4}
Co/TPAA/I_2 (1 redox peak)	0.415*	9.130×10^{-3}	0.094#	0.321	-6.175×10^{-4}
Co/TPAA/I_2 (2 redox peak)	0.699*	3.189×10^{-4}	0.529#	0.170	-2.019×10^{-4}

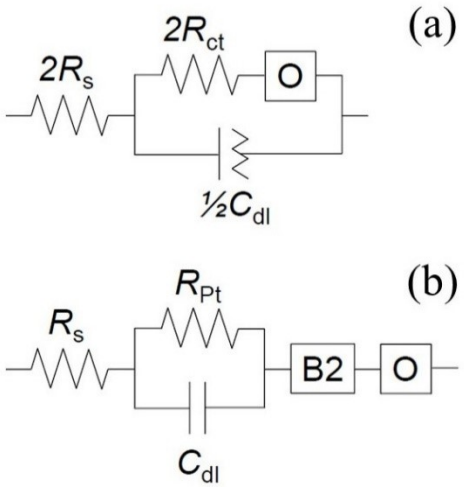

Figure S2. Equivalent circuits used to fit the EIS curves of (a) dummy cells and (b) DSSCs.

The equivalent circuit models used to fit the EIS data (Figure S2) were selected based on the characteristic features of the Nyquist plots and the known electrochemical processes in dye-sensitized solar cells. The series resistance (R_s) accounts for the resistance of the FTO substrate, electrolyte, and contacts, while the charge-transfer resistance (R_{ct}) represents the interfacial redox reaction at the electrode–electrolyte interface. The capacitance element (Cdl) corresponds to the double-layer capacitance associated with charge accumulation at the interface. For symmetric cells, the use of $2R_s$ and $2R_{ct}$ reflects contributions from both identical electrodes. The fitting was performed using complex nonlinear least-squares (CNLS) analysis implemented in ZView software, and the selected circuit provided excellent agreement with the experimental data over the entire frequency range, with low fitting errors (χ^2). These results confirm that the chosen equivalent circuit adequately describes the dominant interfacial charge-transfer processes without requiring additional elements.

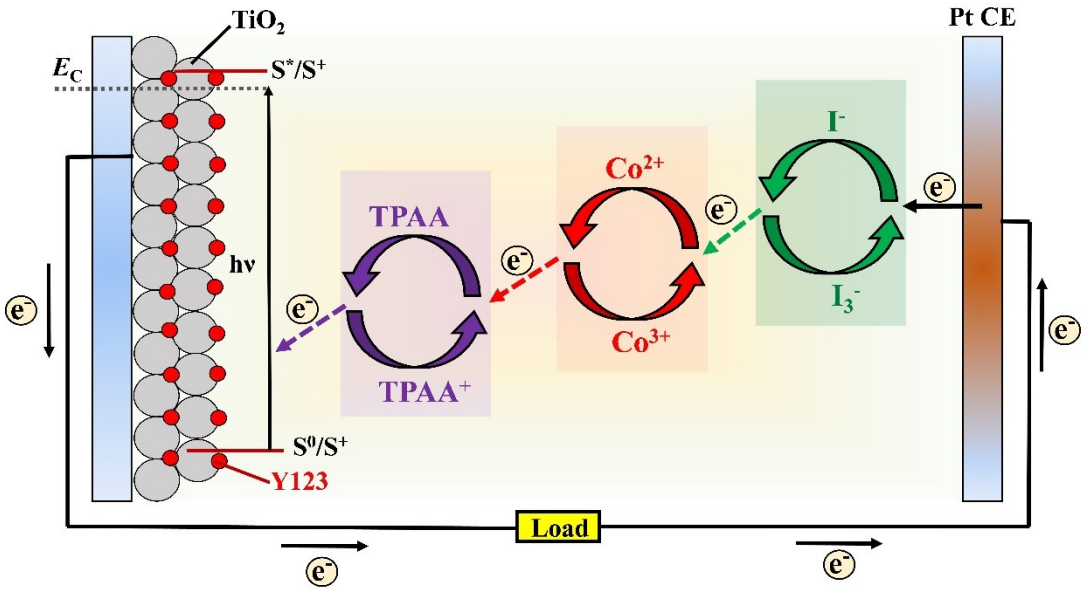

Figure S3. Cascade electron transfer in a ternary TPAA/Co/I_2 electrolyte for DSSCs, illustrating stepwise redox cycling of TPAA/TPAA$^+$, Co^{2+}/Co^{3+}, and I^-/I_3^- between the TiO_2 photoanode and Pt counter electrode.

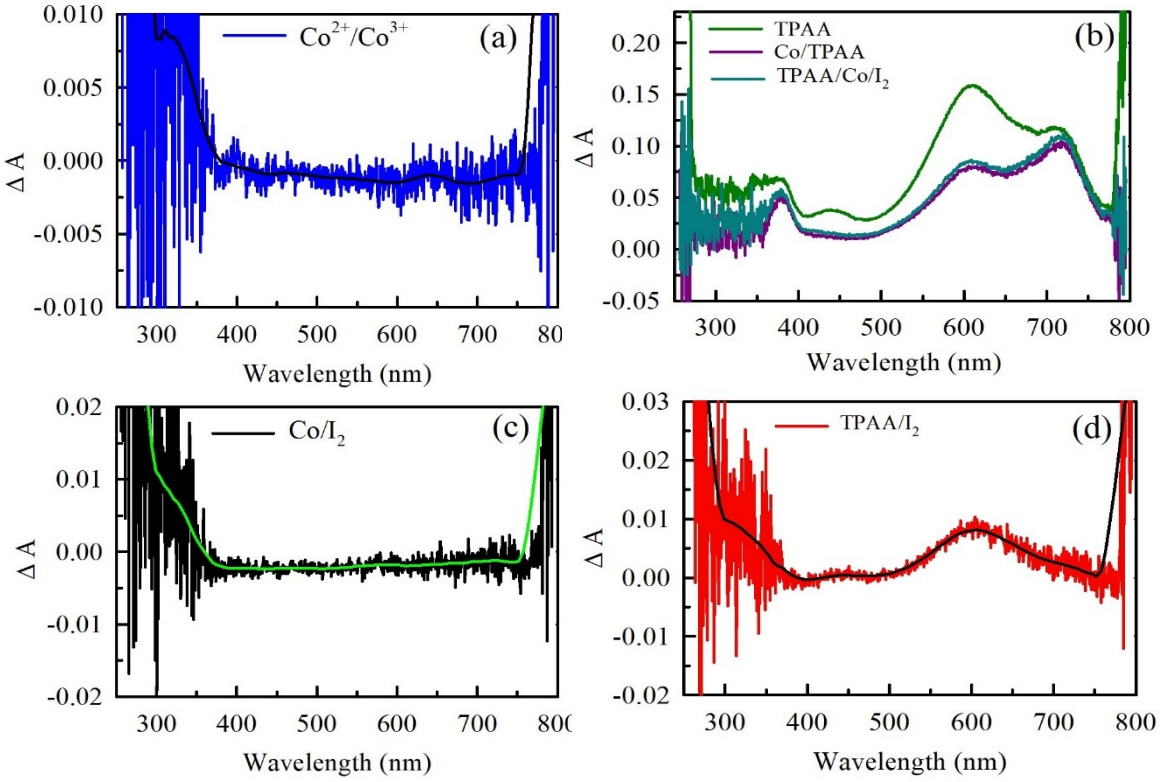

Figure S4. Transient absorption spectroscopy measurements for the electrolytes containing Co^{2+}/Co^{3+}(a), TPAA, Co/TPAA, Co/TPAA/I_2 (b), TPAA/ I_2 (c). (Dye/TiO_2 free system). The Co^{2+}/Co^{3+} couple exhibits negligible spectral variation, indicating minimal intrinsic absorption changes. In contrast, TPAA displays characteristic absorption features that undergo slight modulation upon coordination with cobalt, suggesting weak TPAA–Co interaction. The addition of iodine, more pronounced spectral changes are observed, particularly in TPAA-containing systems, indicative of charge-transfer interactions. The Co/I_2 system shows comparatively weak interaction, whereas the TPAA/I_2 system exhibits significant enhancement in the visible region, confirming strong electronic coupling between TPAA and iodine species. These results reveal the dominant role of TPAA in governing intermolecular interactions within the electrolyte system.

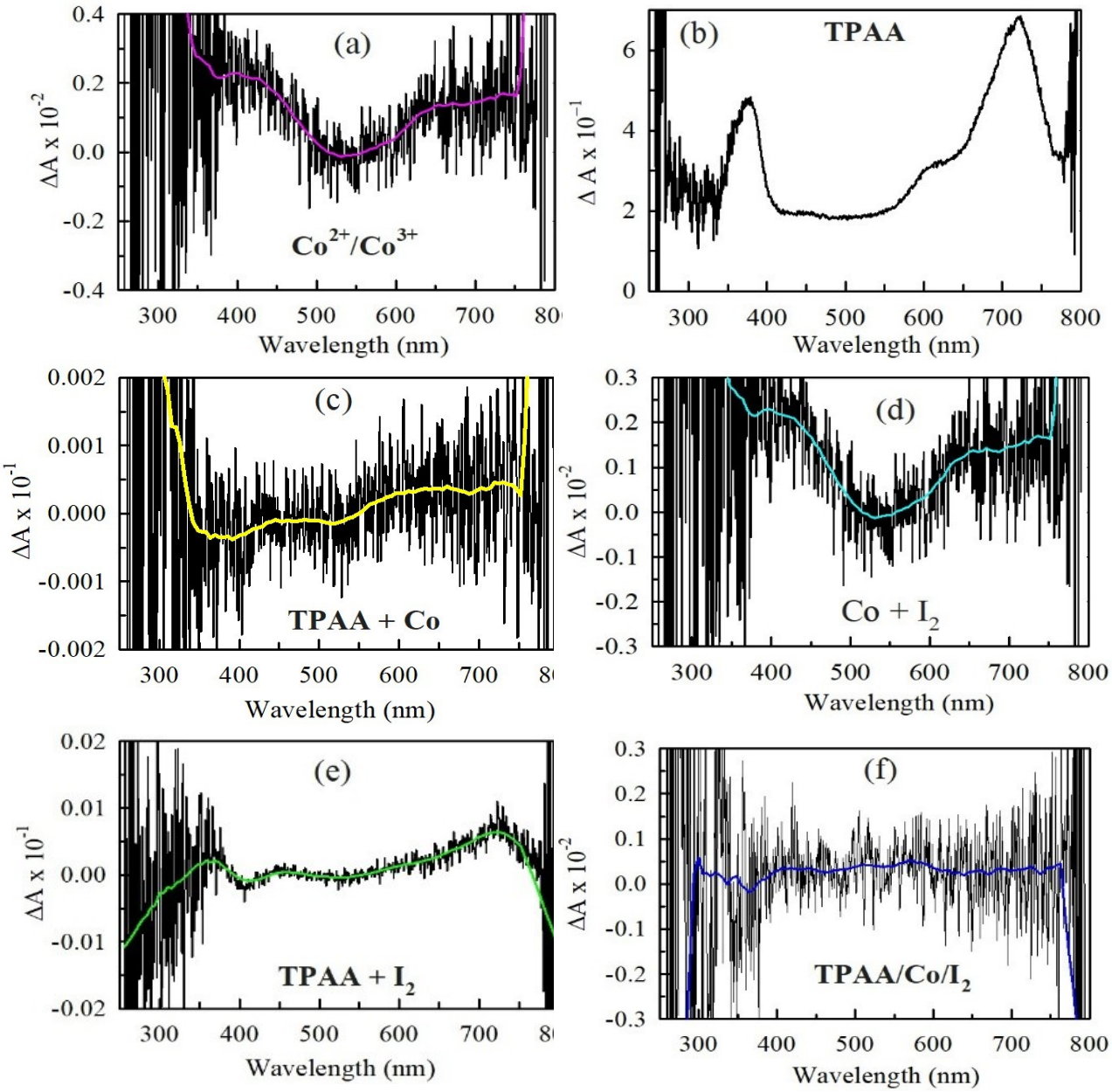

Figure S5. Transient absorption spectra (TAS) of Y123-sensitized TiO_2 photoelectrodes with different electrolyte compositions in acetonitrile: (a) Co^{2+}/Co^{3+}, (b) TPAA, (c) Co/TPAA, (d) Co/I_2, (e) $TPAA/I_2$, and (f) $Co/TPAA/I_2$. The Co^{2+}/Co^{3+} system (a) shows only small changes in the signal, suggesting weak interaction with the excited dye. TPAA alone (b) gives clear spectral features, which change slightly after adding cobalt (c), indicating some interaction between TPAA and Co species. The Co/I_2 system (d) shows moderate changes, while stronger changes are observed for $TPAA/I_2$ (e), pointing to a stronger interaction between TPAA and iodine. For the combined $Co/TPAA/I_2$ system (f), the signal becomes more stable and less intense, suggesting improved charge transfer and better interaction among the components. These results show that TPAA and iodine together influence the charge-transfer behavior at the TiO_2/dye interface.

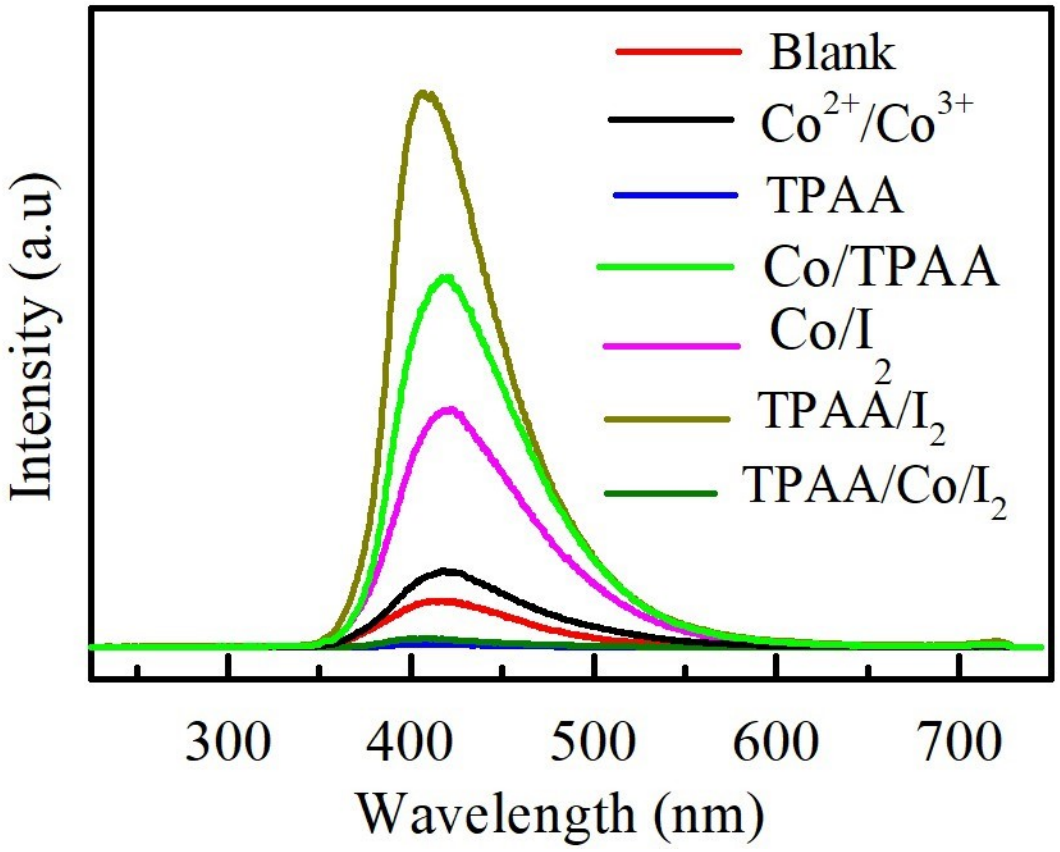

Figure S6. Photoluminescence (PL) spectra of Y123-sensitized TiO_2 in the presence of different electrolyte compositions: blank (Y123/TiO_2), Co^{2+}/Co^{3+}, TPAA, Co/TPAA, Co/I_2, TPAA/I_2, and Co/TPAA/I_2. The blank sample shows relatively low PL intensity, while the addition of Co^{2+}/Co^{3+} and TPAA leads to changes in emission intensity, indicating interaction with the excited dye. The Co/I_2 system shows a moderate increase in PL intensity, whereas TPAA/I_2 exhibits a much stronger emission, suggesting enhanced radiative recombination. In contrast, the Co/TPAA and Co/TPAA/I_2 systems show significantly quenched PL signals, indicating more efficient charge transfer and reduced recombination. Overall, the results suggest that the combined Co/TPAA/I_2 electrolyte promotes better charge separation at the TiO_2/dye interface.

2. NMR analysis for the ion pair formation

1) **TPAA:** ^{1}H NMR (500 MHz, CD_3CN, 300 K) δ 6.91–6.66 (m, Ar–H), 2.13–1.79 (m, CH_3). ^{19}F NMR (470 MHz, CD_3CN, 300 K): No fluorine resonance observed.
2) **Co^{2+} complex:** ^{1}H NMR (500 MHz, CD_3CN, 300 K) δ 14.55–14.38 (br, 1H, bpy–H), 8.66–8.41 (br), 7.39 (br); signals broadened due to paramagnetic Co^{2+}. Residual solvent peak at δ 1.94. ^{19}F NMR δ −72.4 (d, J ≈ 700 Hz, PF_6^-).
3) **Co^{3+} complex:** ^{1}H NMR δ 8.68–8.60, 8.55–8.45, 7.75–7.66, 7.32–7.25. Residual solvent at δ 1.94. ^{19}F NMR δ −73.3 (d, PF_6^-); minor signal at δ ≈ −153 ppm.

4) 4. **Co^{2+}/Co^{3+} mixture:** ^{1}H NMR δ 8.66–8.58, 8.55–8.45, 7.78–7.70, 7.45–7.25, 14.36 (br, trace). ^{19}F NMR δ −73.6 (d, PF_6^-); minor signal at δ ≈ −153 ppm.
5) **Co^{2+}/TPAA mixture:** ^{1}H NMR δ 14.39 (br), 8.68–6.80 (m), 2.12–1.79 (m); broadened due to paramagnetism. ^{19}F NMR δ −73.5 (d, PF_6^-). PF_6^- behaves as outer-sphere counterions.
6) **Co^{3+}/TPAA mixture:** ^{1}H NMR δ 8.68–8.58, 8.53–8.45, 7.73–7.63, 7.30–7.10, 2.10–1.79; weak signal at 14.38 ppm. ^{19}F NMR δ −73.5 (d, PF_6^-). No significant ion-pair differentiation.
7) **Co^{2+}/Co^{3+}/TPAA mixture:** ^{1}H NMR δ 14.38 (br), 8.68–8.60, 8.55–8.45, 7.80–7.65, 7.45–7.25, 6.95–6.70, 2.12–1.88. ^{19}F NMR δ −73.5 (d, PF_6^-). Dynamic outer-sphere ion pairing.
8) **Co^{2+}/I_2 system:** ^{1}H NMR δ 14.39 (br), aromatic signals retained. ^{19}F NMR δ −73.5 (d, PF_6^-). Weak outer-sphere interaction.
9) **Co^{3+}/I_2 system:** ^{1}H NMR similar to Co^{3+} complex. ^{19}F NMR: multiple resonances (−73 to −179 ppm). Indicates multiple PF_6^- environments due to iodine interaction.
10) **Co^{2+}/Co^{3+}/I_2 system:** ^{1}H NMR δ 14.39 (br, trace), 8.68–8.60, 8.55–8.45, 7.78–7.65, 7.45–7.25. ^{19}F NMR δ −34.14, −69.49, −72.42, −73.42, −74.56, −85.35, −116.14, −117.65, −135.91, −152.54, −152.60, −196.55, −199.45, −211.91, −213.29 ppm. ^{1}H signals remain observable, indicating dominance of diamagnetic Co^{3+} species with minor paramagnetic contributions from Co^{2+}. Wide ^{19}F dispersion confirms diverse ion-pair and mixed-valent environments.
11) **TPAA/I_2 system**: ^{1}H NMR: no resolved signals. ^{19}F NMR: no observable signals. Complete radical formation.
12) **Co^{2+}/TPAA/I_2 system**: ^{1}H NMR δ 14.39 (br), 8.70–8.55, 8.50–8.40, 7.80–7.65, 7.45–7.25, 2.13–1.80. ^{19}F NMR δ −18.05, −73.10, −73.69, −75.68, −88.96, −115.61, −127.43, −127.67, −172.21 ppm. Partial suppression of radical formation; equilibrating Co–TPAA–I species.
13) **Co^{3+}/TPAA/I_2 system**: ^{1}H NMR δ 8.68–8.60, 8.55–8.45, 7.78–7.66, 7.32–7.25, 2.13–1.93. ^{19}F NMR δ −21.48, −73.08, −73.59, −73.82, −74.01, −74.31, −74.58, −95.05, −98.04, −107.61, −115.17, −150.31, −152.60, −152.65, −165.88 ppm. Dynamic equilibria with iodine interaction.
14) **Co^{2+}/Co^{3+}/TPAA/I_2 system:** ^{1}H NMR δ 14.38 (br), 8.68–8.60, 8.55–8.45, 7.78–7.65, 7.45–7.25, 2.12–1.90. ^{19}F NMR δ −10.38, −9.58, −73.06, −73.57, −73.78, −74.03, −75.15, −95.19, −99.88, −116.42, −123.55, −145.29, −152.54, −152.59 ppm.Mixed-valet system with dynamic ion pairing and partial radical suppression.

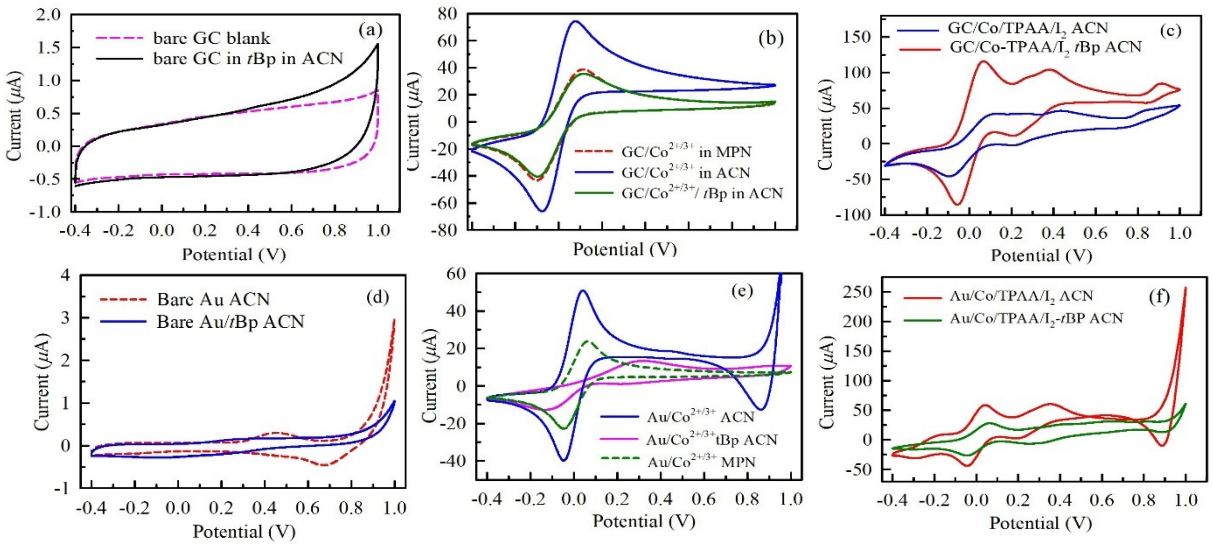

Figure S7. Cyclic voltammograms of different electrolyte systems recorded on glassy carbon (GC) and gold (Au) electrodes. (a) Background voltammograms of bare GC in blank electrolyte and in acetonitrile (ACN) containing *t*-butylpyridine (*t*BP). (b) CV responses of the cobalt redox electrolyte on GC in ACN, MPN, and ACN with tBP. (c) Cyclic voltammograms of GC in the Co/TPAA/I_2 electrolyte in ACN and ACN containing tBP. (d) Background voltammograms of bare Au in ACN and ACN with tBP. (e) CV responses of the cobalt electrolyte on Au in ACN, ACN containing tBP, and MPN. (f) Cyclic voltammograms of Au in the Co/TPAA/I_2 electrolyte in ACN and ACN containing tBP. Measurements were performed within a potential window of −0.4 to 1.0 V at a constant scan rate.

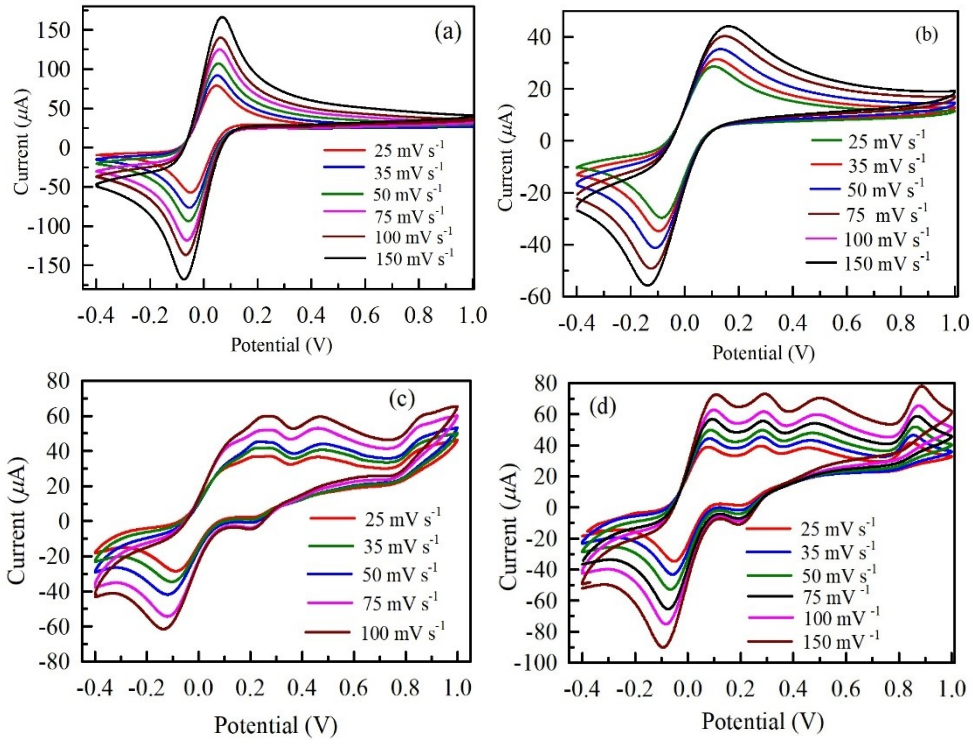

Figure S8. Cyclic voltammograms recorded at different scan rates (25–115 mV s^{-1}) for cobalt-based electrolytes on the GC electrode. (a) Co electrolyte in ACN, (b) Co electrolyte in MPN, (c) Co/TPAA/I_2 electrolyte in ACN, and (d) Co/TPAA/I electrolyte in MPN.

Table S2. Cyclic voltammetry parameters of the Co^{2+}/Co^{3+} redox couple at different scan rates in ACN

Scan Rate (V s^{-1})	√v	E_{pa} (V)	I_{pa} (A)	E_{pc} (V)	I_{pc} (A)
0.025	0.158	0.046	7.683×10^{-5}	−0.046	-7.291×10^{-5}
0.035	0.187	0.047	9.002×10^{-5}	−0.051	-8.650×10^{-5}
0.050	0.224	0.052	1.046×10^{-4}	−0.054	-1.014×10^{-4}
0.075	0.274	0.058	1.278×10^{-4}	−0.059	-1.222×10^{-4}
0.100	0.316	0.060	1.456×10^{-4}	−0.064	-1.381×10^{-4}
0.115	0.339	0.065	1.688×10^{-4}	−0.070	-1.645×10^{-4}

(GC carbon electrode).

Table S3. Cyclic voltammetry parameters of the Co^{2+}/Co^{3+} redox couple in MPN at different scan rates.

Scan Rate (V s^{-1})	√v	E_{pa} (V)	I_{pa} (A)	E_{pc} (V)	I_{pc} (A)
0.025	0.158	0.102	2.909×10^{-5}	−0.080	-2.865×10^{-5}
0.035	0.187	0.111	3.179×10^{-5}	−0.090	-3.230×10^{-5}
0.050	0.224	0.124	3.815×10^{-5}	−0.102	-3.643×10^{-5}
0.075	0.274	0.134	3.996×10^{-5}	−0.118	-4.000×10^{-5}
0.100	0.316	0.144	4.400×10^{-5}	−0.128	-4.157×10^{-5}
0.115	0.339	0.149	4.848×10^{-5}	−0.128	-4.529×10^{-5}

Table S4. Cyclic voltammetry parameters of the Co/TPAA/I_2 system in ACN at different scan rates.

Scan Rate (V s^{-1})	√v	E_{pa} (V)	I_{pa} (A)	E_{pc} (V)	I_{pc} (A)
0.025	0.158	0.044	1.032×10^{-4}	−0.063	-9.478×10^{-5}
0.035	0.187	0.048	1.186×10^{-4}	−0.067	-1.106×10^{-4}
0.050	0.224	0.054	1.394×10^{-4}	−0.073	-1.266×10^{-4}
0.075	0.274	0.060	1.620×10^{-4}	−0.081	-1.509×10^{-4}
0.100	0.316	0.067	1.794×10^{-4}	−0.089	-1.467×10^{-4}
0.150	0.339	0.075	2.133×10^{-4}	−0.102	-1.987×10^{-4}

Scan Rate (V s^{-1})	√v	E_{pa} (V)	I_{pa} (A)	E_{pc} (V)	I_{pc} (A)
0.025	0.158	0.060	2.138×10^{-5}	−0.049	-3.020×10^{-5}
0.035	0.187	0.065	2.462×10^{-5}	−0.053	-3.524×10^{-5}
0.050	0.224	0.070	2.818×10^{-5}	−0.060	-4.126×10^{-5}
0.075	0.274	0.073	3.323×10^{-5}	−0.070	-4.895×10^{-5}
0.100	0.316	0.077	3.528×10^{-5}	−0.077	-5.507×10^{-5}

0.115	0.339	0.083	4.012×10^{-5}	−0.089	-6.419×10^{-5}

Table S5. Cyclic voltammetry parameters of the Co/TPAA/I_2 system in MPN at different scan rates.

Diffusion coefficient calculation using Randles–Ševčík Equation (25 °C)

$$I_p = 2.69 \times 10^5 \, n^{3/2} \, A \, C \, D^{1/2} \, \nu^{1/2}$$

Where *I*p = peak current (A), n = number of electrons transferred (1 for Co^{3+}/Co^{2+}), A = electrode area (cm^2), C = concentration (mol cm^{-3}), D = diffusion coefficient (cm^2 s^{-1}), ν = scan rate (V s^{-1}). A linear relationship between Ip and the square root of the scan rate √ν was observed, confirming diffusion-controlled redox behaviour. The diffusion coefficients were calculated from the slopes of the *I*p versus √ν plots.

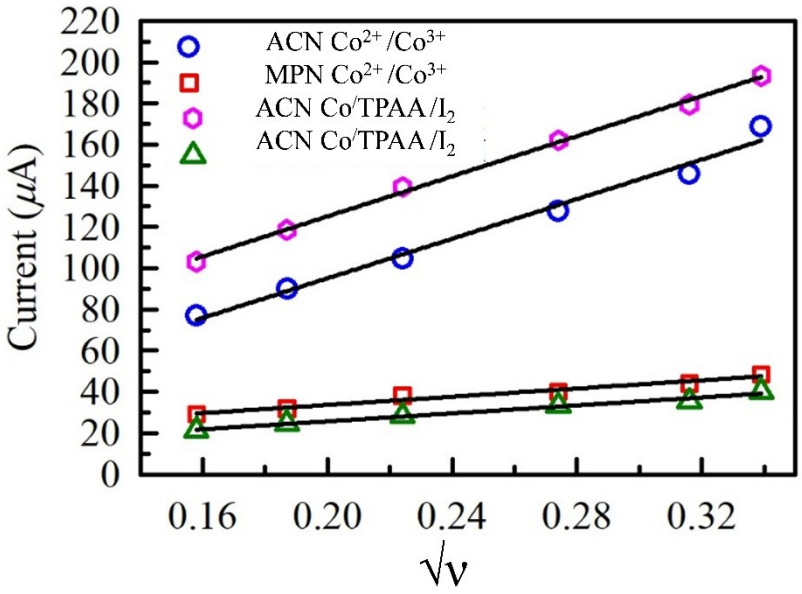

Figure S9. Dependence of peak current on the square root of scan rate for cobalt redox electrolytes in different solvent systems. The plot shows the linear relationship between the peak current (μA) and the square root of scan rate (√ν) for ACN Co(II)/Co(III), MPN Co(II)/Co(III), ACN Co–TPAA–I, and MPN Co–TPAA–I electrolytes.

The slopes obtained from the linear fits are 4.807×10^{-4} (ACN–cobalt), 9.95×10^{-5} (MPN–cobalt), 4.869×10^{-4} (ACN–Co–TPAA–I), and 9.656×10^{-5} (MPN–Co–TPAA–I). For the Co^{3+}/Co^{2+} redox couple, n = 1, and a GC electrode with an area of 0.071 cm^2 (3 mm diameter) was used. The concentrations of Co^{2+} and Co^{3+} were 7.33×10^{-3} M and 1.66×10^{-3} M, respectively, giving a total concentration of 8.99×10^{-3} M (8.99×10^{-6} mol cm^{-3}). A linear relationship between Ip and √ν was observed, confirming diffusion-controlled redox behavior. The diffusion coefficients were determined from the slopes of the I_p versus √ν plots using $D = (\text{slope} / (2.69 \times 10^5 \, n^{(3/2)} \, A \, C))^2$. The calculated diffusion coefficients were 7.84×10^{-6} and 3.36×10^{-7} $cm^2 \, s^{-1}$ for the Co^{2+}/Co^{3+} system in ACN and MPN, respectively, and 8.04×10^{-6} and 3.16×10^{-7} $cm^2 \, s^{-1}$ for the Co–TPAA–I system in ACN and MPN, respectively.

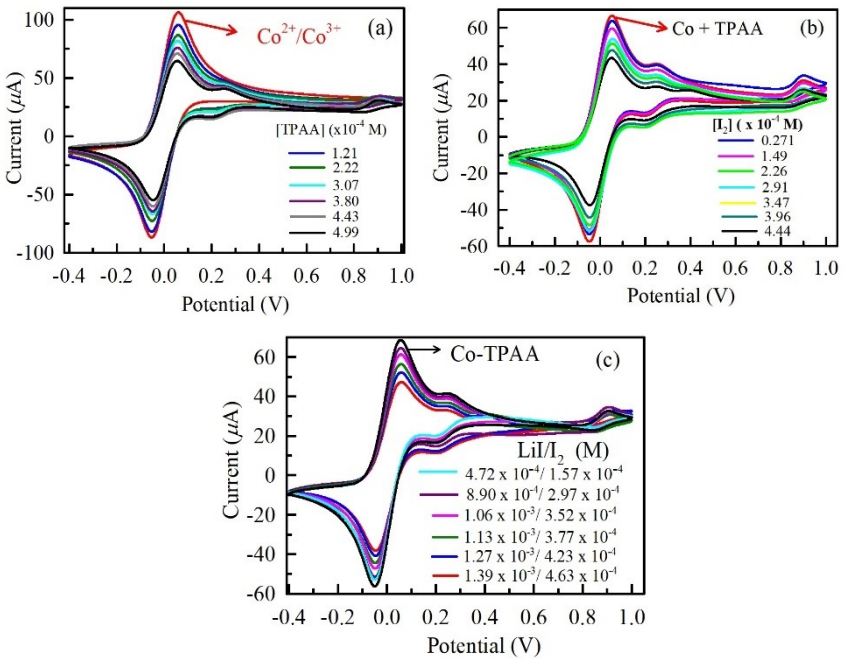

Figure S10. Cyclic voltammograms recorded at a GC electrode illustrating the electrochemical behavior of the cobalt–TPAA–iodine electrolyte system in acetonitrile: (a) effect of TPAA concentration on the Co^{2+}/Co^{3+} redox couple, (b) influence of iodine concentration on the Co–TPAA system, and (c) effect of LiI/I_2 composition on the electrochemical response of the Co–TPAA electrolyte.

The cyclic voltammograms show a gradual decrease in the anodic and cathodic peak currents with increasing concentration of the added species. In Figure S9a, the addition of TPAA to the Co^{2+}/Co^{3+} electrolyte leads to a systematic reduction in peak currents, indicating interaction between TPAA and the cobalt redox couple. In Figure S9b, further addition of iodine to the Co/TPAA system results in a more pronounced decrease in current, suggesting stronger interactions involving iodine species. A similar trend is observed in Figure S9c upon addition of LiI/I_2, where the redox response continues to decrease with increasing concentration. The continuous suppression of peak currents indicates the formation of interacting species in solution, which hinder the diffusion of cobalt ions to the electrode surface. These results support the presence of weak ion-pair interactions in the electrolyte system.

Table S6. CV parameters of the Co^{2+}/Co^{3+} redox couple in the presence of varying concentrations of TPAA in acetonitrile.

TPAA (x 10^{-4} M)	E_{pa} (V)	E_{pc} (V)	Δ_{Ep} (V)	I_{pa} (A)	I_{pc} (A)	I_{pa}/I_{pc}
***Co electrolyte**	0.056	-0.051	0.005	9.937×10^{-5}	-9.185×10^{-5}	1.08
1.21	0.052	-0.051	0.103	1.022×10^{-4}	-9.957×10^{-5}	1.03
2.22	0.051	-0.047	0.098	6.717×10^{-5}	-8.229×10^{-5}	0.82
3.07	0.050	-0.047	0.097	6.205×10^{-5}	-7.654×10^{-5}	0.81
3.80	0.048	-0.046	0.094	5.690×10^{-5}	-7.130×10^{-5}	0.80
4.43	0.047	-0.044	0.091	5.260×10^{-5}	-6.717×10^{-5}	0.78
4.99	0.045	-0.044	0.089	4.861×10^{-5}	-6.751×10^{-5}	0.72

*$Co(bpy)_3(PF_6)_2$ 7.33×10^{-3} M, $Co(bpy)_3(PF_6)_3$ 1.666×10^{-3} M

Table S7. Current–ratio analysis for binding constant determination of TPAA with the Co redox couple.

TPAA (M)	I_{pa} (A)	I_0/I	$(I_0/I - 1)$
4.50×10^{-5}	6.717×10^{-5}	1.48	0.48
1.83×10^{-4}	6.205×10^{-5}	1.60	0.60
3.07×10^{-4}	5.690×10^{-5}	1.75	0.75
3.80×10^{-4}	5.260×10^{-5}	1.89	0.89
4.99×10^{-4}	4.861×10^{-5}	2.04	1.04

Table S8. Cyclic voltammetric parameters of the Co-TPAA system in the presence of increasing

No.	Volume (μL)	I_2 (M)	E_{pa} (V)	E_{pc} (V)	ΔE_p (V)	I_{pa} (A)	I_{pc} (A)	I_{pa}/I_{pc}
1	50	5.52×10^{-6}	0.045	-0.044	0.089	4.951×10^{-5}	-6.204×10^{-5}	0.80
2	250	2.71×10^{-5}	0.044	-0.045	0.089	4.793×10^{-5}	-6.030×10^{-5}	0.79
3	1550	1.49×10^{-4}	0.044	-0.044	0.088	4.483×10^{-5}	-5.666×10^{-5}	0.79
4	2570	2.26×10^{-4}	0.044	-0.044	0.088	4.259×10^{-5}	-5.333×10^{-5}	0.80
5	3550	2.91×10^{-4}	0.047	-0.044	0.091	4.001×10^{-5}	-5.080×10^{-5}	0.79
6	4550	3.47×10^{-4}	0.044	-0.044	0.088	3.744×10^{-5}	-4.773×10^{-5}	0.78
7	5550	3.96×10^{-4}	0.043	-0.045	0.088	3.627×10^{-5}	-4.553×10^{-5}	0.80
8	6650	4.44×10^{-4}	0.041	-0.041	0.082	3.342×10^{-5}	-4.100×10^{-5}	0.82

iodine (I_2) concentration.

Table S9. Current–ratio analysis for binding constant determination of I_2 with the Co-TPAA

I_2 (M)	I_{pa} (A)	I_0/I	$(I_0/I - 1)$
5.52×10^{-6}	4.951×10^{-5}	1.000	0.000
2.71×10^{-5}	4.793×10^{-5}	1.033	0.033
1.49×10^{-4}	4.483×10^{-5}	1.104	0.104
2.26×10^{-4}	4.259×10^{-5}	1.162	0.162
2.91×10^{-4}	4.001×10^{-5}	1.237	0.237
3.47×10^{-4}	3.744×10^{-5}	1.323	0.323
3.96×10^{-4}	3.627×10^{-5}	1.365	0.365
4.44×10^{-4}	3.342×10^{-5}	1.481	0.481

system.

Table S10. Cyclic voltammetric parameters of the Co-TPAA system in the presence of varying

Volume (µL)	LiI (M)	I_2 (M)	E_{pa} (V)	E_{pc} (V)	ΔE_p (V)	I_{pa} (A)	I_{pc} (A)	I_{pa} / I_{pc}
50	1.66×10^{-5}	5.52×10^{-6}	0.048	-0.047	0.095	4.987×10^{-5}	-6.328×10^{-5}	0.79
400	1.28×10^{-4}	4.27×10^{-5}	0.047	-0.047	0.094	4.850×10^{-5}	-6.119×10^{-5}	0.79
1650	4.72×10^{-4}	1.57×10^{-4}	0.047	-0.044	0.091	4.459×10^{-5}	-5.669×10^{-5}	0.79
3650	8.90×10^{-4}	2.97×10^{-4}	0.048	-0.045	0.093	4.107×10^{-5}	-5.271×10^{-5}	0.78
4650	1.06×10^{-3}	3.52×10^{-4}	0.048	-0.044	0.092	3.817×10^{-5}	-4.953×10^{-5}	0.77
5150	1.13×10^{-3}	3.77×10^{-4}	0.047	-0.043	0.090	3.581×10^{-5}	-4.696×10^{-5}	0.76
6150	1.27×10^{-3}	4.23×10^{-4}	0.047	-0.044	0.091	3.491×10^{-5}	-4.590×10^{-5}	0.76
7150	1.39×10^{-3}	4.63×10^{-4}	0.048	-0.044	0.092	3.324×10^{-5}	-4.320×10^{-5}	0.77

concentrations of LiI and I_2

Table S11. Current–ratio analysis for the interaction between iodine (I_2) and the Co-TPAA redox

I_2 (M)	I_{pa} (A)	I_0/I	$(I_0/I - 1)$
1.57×10^{-4}	4.459×10^{-5}	1.09	0.09
2.97×10^{-4}	4.107×10^{-5}	1.18	0.18
3.52×10^{-4}	3.817×10^{-5}	1.27	0.27
3.77×10^{-4}	3.581×10^{-5}	1.36	0.36
4.23×10^{-4}	3.491×10^{-5}	1.39	0.39
4.63×10^{-4}	3.324×10^{-5}	1.46	0.46

system.

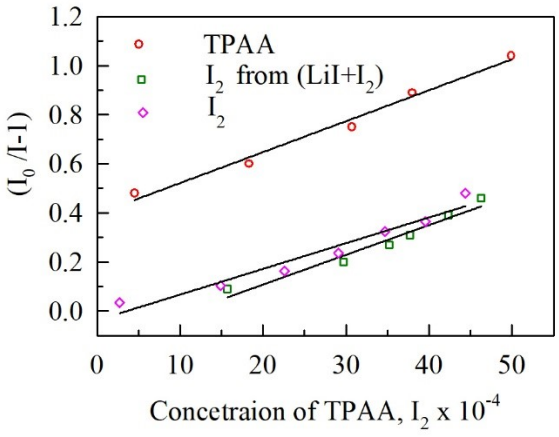

Figure S11. Linear regression plots of (I_0/I−1) as a function of ligand concentration for TPAA, iodine generated from the LiI/I_2 electrolyte, and molecular I_2.

A plot of (I_0/I − 1) versus TPAA concentration exhibits a linear relationship consistent with the equation y = Kx + b, where the slope corresponds to the binding constant (K). The calculated binding constants were 1.26 × 10^3 M^{-1} for the Co–TPAA system, 1.04 × 10^3 M^{-1} for the Co–TPAA system in the presence of LiI/I_2, and 1.19 × 10^3 M^{-1} for the Co–TPAA–I_2 system.

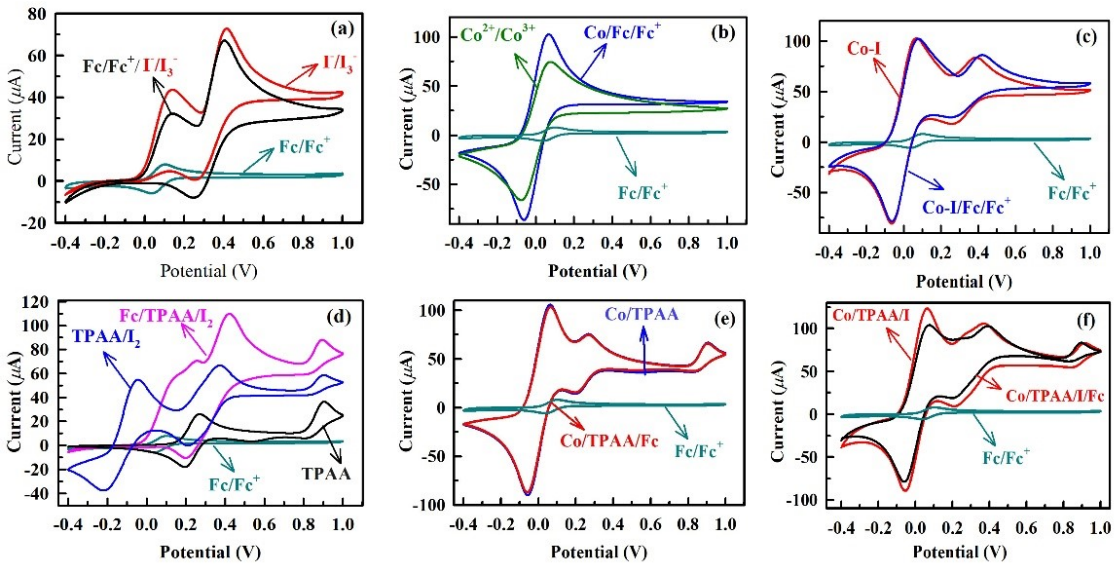

Figure S12. Cyclic voltammograms recorded in acetonitrile using ferrocene (Fc/Fc^+) as an internal redox probe for different electrolyte systems: (a) Fc/Fc^+ with I^-/I_3^-, (b) Co^{2+}/Co^{3+} and $Co/Fc/Fc^+$, (c) Co/I_2 and $Co/I_2/Fc/Fc^+$, (d) TPAA, $TPAA/I_2$, and $Fc/TPAA/I_2$, (e) Co/TPAA and $Co/TPAA/Fc/Fc^+$, and (f) $Co/TPAA/I_2$ and $Co/TPAA/I_2/Fc/Fc^+$.

In detail, Figure S11a shows well-resolved Fc/Fc^+ peaks alongside the I^-/I_3^- redox couple. In Figure S11b, the Co^{2+}/Co^{3+} redox peaks dominate, resulting in partial suppression of the Fc signal. A similar trend is observed in Figure S11c for the Co/ I_2 system, where overlapping redox processes further reduce the visibility of Fc/Fc^+. In Figure S11d, the presence of TPAA and $TPAA/I_2$ introduces additional redox features, leading to further attenuation of the Fc response. For the Co/TPAA system (Figure S11e), the cobalt redox peaks remain dominant, while in the ternary $Co/TPAA/I_2$ system (Figure S11f), the Fc/Fc^+ signal is almost completely suppressed. The progressive disappearance of the Fc/Fc^+ peaks indicates the absence of strong inner-sphere coordination and supports an outer-sphere electron-transfer mechanism.

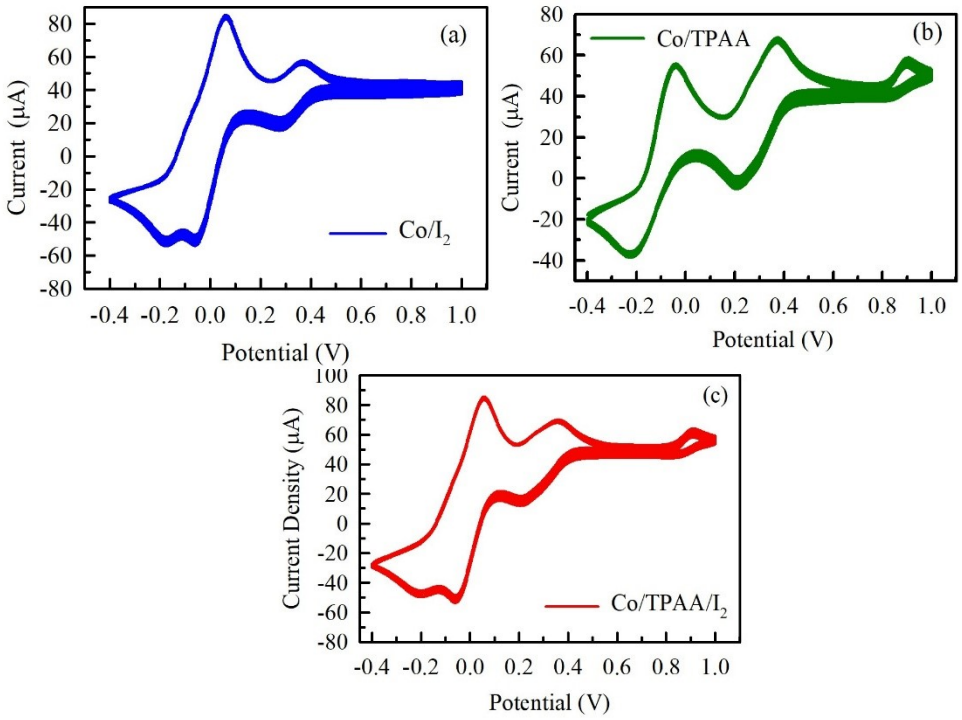

Figure S13. Electrochemical stability of Co/I, Co/TPAA, and Co/TPAA/I_2 electrolytes evaluated over 50 cyclic CV cycles using a Pt electrode.

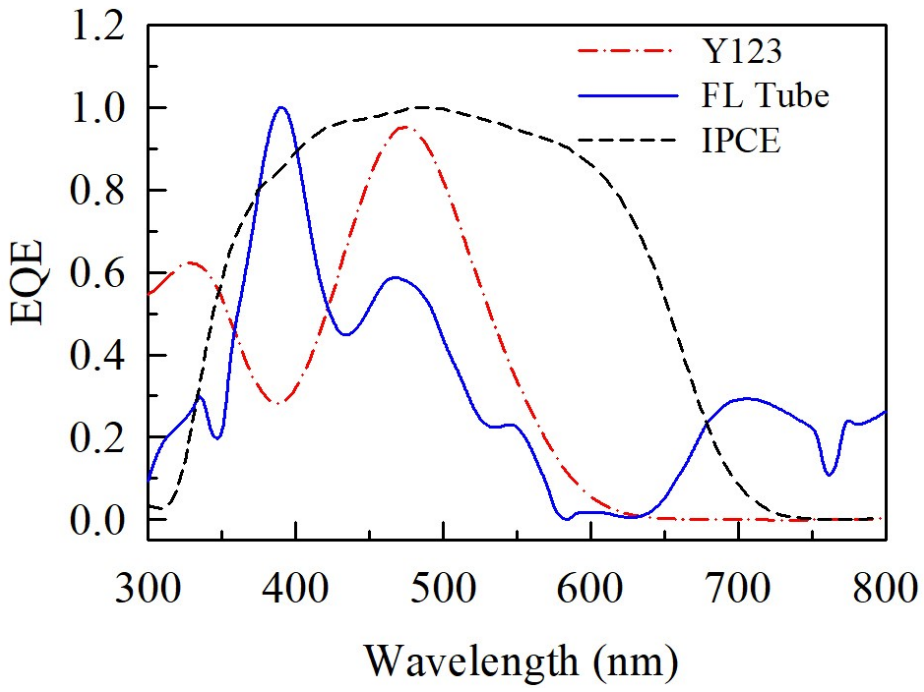

Figure S14. Normalized emission spectrum of the fluorescent light source, EQE spectrum of the Y123-based DSSC, and absorption spectrum of Y123 dye in ACN, showing good overlap in the 400–550 nm region and reduced response above 600 nm.

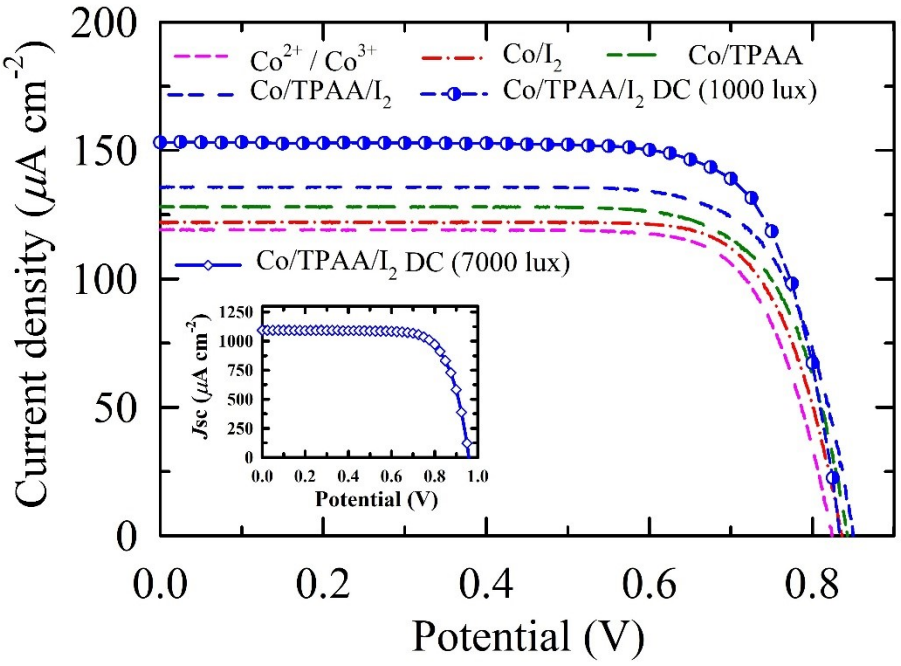

Figure S15. J–V curves of DSSCs with a sandwich structure employing (i) iodide electrolytes, (ii) cobalt electrolytes, (iii) cobalt electrolytes with TPAA, and (iv) cobalt electrolytes with TPAA and iodine under 1000 lux room-light illumination. J–V curves of DSSCs with a direct contact structure using cobalt electrolytes with TPAA under 1000 and 7000 lux (inset) room-light illumination are also shown.

Table S12. Comparison of dye-sensitized solar cells employing dual and ternary redox couples under 1-sun condition

Work (Year)	Redox Couples / Additives	Architecture	Dye	PCE (1-sun)
This work (2025) – direct contact	$Co(bpy)_3^{2+/3+}$/ TPAA/I^-/I_3^- (ternary ion-pair)	Direct-contact	Y123	**11.51%**
This work (2025) – sandwich	$Co(bpy)_3^{2+/3+}$/ TPAA/I^-/I_3^- (ternary ion-pair)	Sandwich	Y123	**10.95%**
Hao et al., Nat. Commun., 2016, 7, 13934.	$Co(bpy)_3^{2+/3+}$/TPAA	Sandwich	LEG4	10.5% (1-sun), 11.7% (0.46-sun)
Ayaz et al., ACS Appl. Energy Mater. 2022, 5, 4240-4246.	I^-/I_3^-/TPAA (0.1 M)	Sandwich	LEG4	5.68%
Cong et al., ChemSus Chem 2015, 8, 264-268.	TEMPO/ $Co(bpy)_3^{2+/3+}$ Double redox couple	Sandwich	LEG4	8.4%
Wang et al. RSC Adv., 2017, 7, 13689.	[BMI] $[Co(NCS)_4]$, Double redox couple	Sandwich	D205	8.1%
Y. Lee et al. J. Ind. Eng. Chem. 2022, 115, 263–271.	MPII/Co FKC209 Double redox couple	Sandwich	N719	9.67
Md.M. Rahman et al. ChemistrySelect 2023, 8, e202300704.	I^-, $Br^-/(I_3^-, I_2Br^-)$ Double redox couple	Sandwich	SA/IAA-	0.57%
J. Cong et al Adv. Energy Mater. 2014, 4, 1301273.	$Co(bpy)_3^{2+/3+}$/ I^-/I_3^-	Sandwich	LEG4	7.5%

Table S13. Performance comparison of indoor photovoltaic devices (DSSCs, OPVs, and PSCs) under ~1000 lux illumination.

Device	System	Light Source	Intensity (lux)	Jsc (μA cm^{-2})	Voc (V)	FF	PCE (%)	Ref.
DSSCs	Co/TPA/I_2-Y123	T5 lamp	1000	15.11	0.834	0.765	30.34	This work
DSSC	(Cu(tmby)$2^{2+/+}$, Y123 + XY1b)	LED (2700 K)	1000	127	0.770	0.836	30.2	S1
DSSC	RJ-C6 + XY1b (dual Cu electrolyte)	CFL (warm white)	1000	—	—	—	37.3	S2
DSSC	Y123:XY1b + Cu(tmby)$2^{2+/+}$	CFL	1000	130.2	0.99	0.757	34.65	S3
DSSC	PEO/PMMA QS-DSSC (Cu(dmby)$2^{2+/+}$)	Fluorescent (6500 K)	1000	134.71	0.917	0.765	30.51	S4
DSSC	Cu-based zombie DSC	Indoor LED/FL	1000	147	0.91	0.77	34.0	S5
DSSC	ITO NT/m-TiO2 (YKP-88)	LED (6500 K)	98	17.6	0.286	0.63	22.6	S6
OPV	DCP-based OPV	LED (2700 K)	1000	126	0.926	0.807	30.4	S7
OPV	PM6:DYO-V	LED (2600 K)	1000	133.1	0.861	0.735	26.5	S8
OPV	PM6:DY6FO-V	LED (2600 K)	1000	131	0.872	0.764	27.5	S9
OPV	BPA / PM6:Y6	LED (2700 K)	1000	165.1	0.668	0.745	28.6	S10
OPV	PM6:Y6-O-iso	LED (2600 K)	1000	120.5	0.870	0.732	24.1	S11
PSC	NiOx/MeO-2PACz	LED (3000 K)	1000	288.45	1.04	0.798	40.09	S12
PSC	PPCI (PCBM doped)	LED	1000	137.81	0.990	0.842	41.05	S13
PSC	$Cs_{0.18}FA_{0.82}Pb(I_{0.8}Br_{0.2})_3$ + PDI	LED (3000 K)	1000	285.75	1.05	0.796	40.72	S14

[S1] K. Sasitharan and M. Freitag, *ACS Appl. Energy Mater.* 2025, **8**, 9891–9899.

[S2] S. M. Meethal, S. C. Pradhan, J. Velore, S. Varughese, R. S. Pillai, F. Sauvage, A. Hagfeldt and S. Soman, *J. Mater. Chem. A* 2024, **12**, 1081–1093.

[S3] A. S. George, T. W. Hamann and S. Soman, *Energy Fuels* 2025, **39**, 4927–4938.

[S4] Y.-H. Lee, S. Venkatesan, X.-W. Wong, Z. Q. Lim, L.-Y. Chang, Y.-L. Lee and K.-C. Ho, *Chem. Eng. J.* 2024, **501**, 157506.

[S5] D. Ivanou and A. M. Mendes, *ACS Appl. Energy Mater.* 2025, **8**, 11021–11032.

[S6] J. Castillo-Seoane, L. Contreras-Bernal, A. J. Riquelme, S. Fauvel, Y. Kervella, J. Gil-Rostra, G. Lozano, A. Barranco, R. Demadrille, J. R. Sánchez-Valencia and A. Borrás, *Mater. Today Energy* 2025, **49**, 101851.

[S7] W. Wang, Y. Cui, Y. Yu, J. Wang, C. Wang, H. Hou, Q. Kang, H. Wang, S. Chen, S. Zhang, H. Xia and J. Hou, *Nano Energy* 2024, **128**, 109893.
[S8] H. M. Ng, B. Zou, A. Sergeev, Y. Fu, P. F. Chan, Z. Yao, Q. Wang, Z. Li, C.-J. Su, U.-S. Jeng, X. Hu, G. Li, X. Lu, K. S. Wong, Z.-G. Zhang, Y. Chen, W.-Y. Wong, H. Yu and H. Yan, *Energy Environ. Sci.* 2025, **18**, 6587–6596.
[S9] B. Zou, H. M. Ng, Z. Li, Y. Wang, Q. Wang, D. Chen, Z. Yao, H. Li, C. Li, X. Zeng, W. Liu, J. E. Halpert, H. Hu, C. Duan, Z. Zhu, T. Wu, W.-Y. Wong, Z.-G. Zhang, H. Yan and H. Yu, *Adv. Sci.* 2025, **12,** e12690.
[S10] S. Wang, S. Wang, J. Wang, N. Yu, J. Qiao, X. Xie, C. Li, M. S. Abbasi, R. Ding, X. Zhang, Y. Han, G. Lu, J. Zhang, X. Hao, Z. Tang, Y. Cai and H. Huang, *Adv. Energy Mater.* 2026, **16**, 2405205.
[S11] L. Xie, H. M. Ng, B. Yu, H. Yu, C. Ga, K. Ding, Z. Qi, H. Ade, G. Zhang, S. H. Pun and H. Yan, *Solar RRL* 2026, **10**, e202500922.
[S12] Z.-E. Shi, T.-H. Cheng, C.-Y. Lung, C.-W. Lin, C.-L. Wang, B.-H. Jiang, Y.-S. Hsiao and C.-P. Chen, *Chem. Eng. J.* 2024, **498**, 155512.
[S13] D. Li, T. Nie, G. Zhao, R. Lv, J. Feng, J. Ding, S. Yang, S. (F.) Liu and Z. Fang, *Adv. Funct. Mater.* 2026, **36**, e02847.
[S14] B. Orwat, Z.-E. Shi, C.-H. Ma, K. Jankowska, J. Nawrocik, A. Singh, Y.-H. Zheng, W.-C. Tu, Z. Ling, P. Dabczyński, M. Rogala, P. Krukowski, P. J. Kowalczyk, P. Data, B. Łuszczynska, I. Kownacki and C.-P. Chen, *Small* 2025, **21**, 2411623.

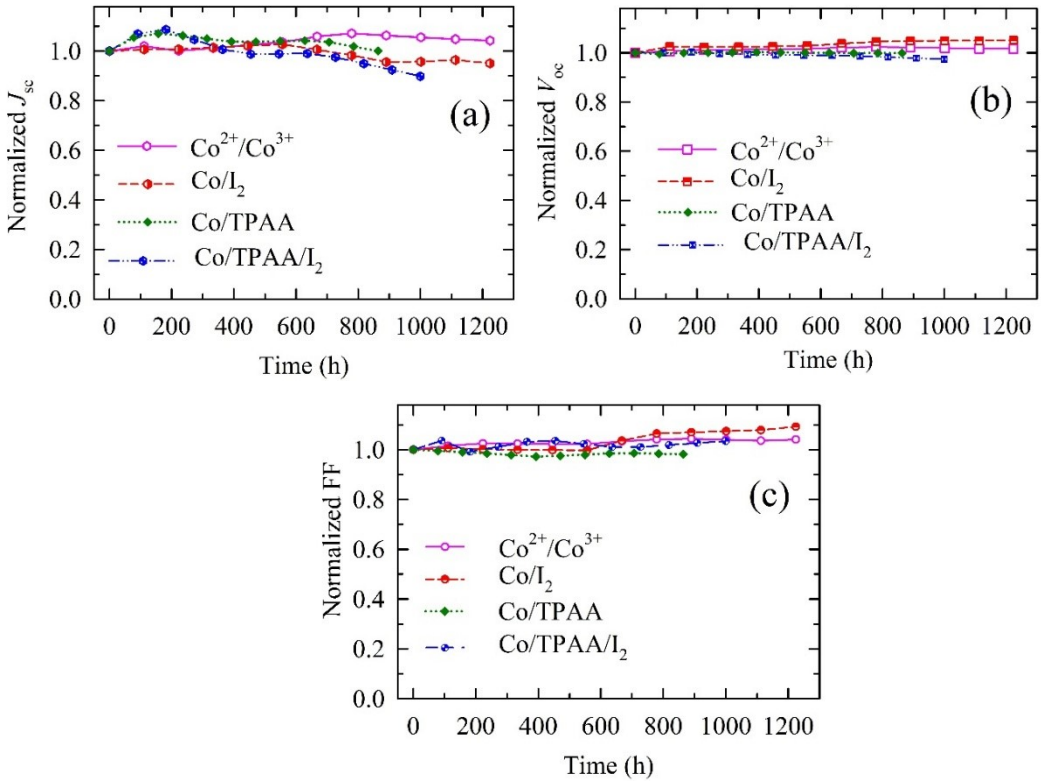

Figure S16. Normalized (a) J_{sc}, (b) V_{oc}, and (c) FF of the DSSCs using Co, Co/I_2, Co/TPAA and Co/TPAA/I_2 complex electrolytes under one-sun conditions.